Supporting Information

A single-ion single-electron cerrous magnet

Sandeep K. Gupta,[a] Swaminathan Shanmugan,[a,b] Thayalan Rajeshkumar,[a] Aditya Borah,[a] Marko Damjanović,[c] Michael Schulze,[c] Wolfgang Wernsdorfer,[c] Gopalan Rajaraman*[a] and Ramaswamy Murugavel*[a]

[a] Department of Chemistry, Indian Institute of Technology Bombay, Mumbai-400076, India. E-mail: rajaraman@chem.iitb.ac.in, rmv@chem.iitb.ac.in

[b] Department of Chemistry, SRM Institute of Science and Technology, Kattankulathur, Kancheepuram 603203, Tamil Nadu, India

[c] Physikalisches Institut, Karlsruhe Institute of Technology (KIT), Wolfgang-Gaede-Strasse 1, 76131 Karlsruhe; Institute of Nanotechnology, KIT, Hermann-von-Helmholz-Platz 1, 76344, Eggenstein-Leopoldshafen, Germany

Table S1. Crystal data and structure refinement details for **1** and **2**.

Identification code	CCDC 1590248	CCDC 1877236
Empirical formula	$C_{30}H_{75}CeN_9O_{12}P_3$	$C_{30}H_{75}LaN_9O_{12}P_3$
Formula weight	987.02	985.81
Temperature	150(2) K	120(2) K
Crystal system	Orthorhombic	Orthorhombic
Space group	*P*bca	*P*bca
a (Å)	26.230(4)	26.322(10)
b (Å)	17.688(2)	17.718(7)
c (Å)	43.297(6)	43.481(2)
Volume ($Å^3$)	20088(5)	20278(2)
Z	16	16
Crystal size (mm^3)	0.37 x 0.06 x 0.02	0.28 x 0.04 x 0.02
Reflections collected	86784	80836
Independent reflections	17326 [R(int) = 0.0351]	17541 [R(int) = 0.1187]
Data / restraints / parameters	17326 / 5 / 1081	17541 / 26 / 1064
Goodness-of-fit on F2	1.185	1.388
Final R indices [I>2sigma(I)]	R1 = 0.0409, wR2 = 0.0750	R1 = 0.1433, wR2 = 0.2423
R indices (all data)	R1 = 0.0446, wR2 = 0.0766	R1 = 0.1581, wR2 = 0.2493
Largest diff. peak and hole (e $Å^{-3}$)	0.808 and -0.586	0.829 and -1.262

Table S2. SHAPE measures for seven co-ordinate Ce(III) center in **1**.[1]

Structure [CeO_9]	Symmetry	Ce1	Ce2
Muffin	C_s	2.786	4.492
Hula-hoop	C_{2v}	7.357	6.298
Tridiminished icosahedron J63	C_{3v}	12.518	10.635
Spherical tricapped trigonal prism	D_{3h}	4.449	5.372
Tricapped trigonal prism J51	D_{3h}	4.7	5.287
Spherical capped square antiprism	C_{4v}	3.385	5.058
Capped square antiprism J10	C_{4v}	4.224	6.006
Spherical-relaxed capped cube	C_{4v}	8.06	6.206
Capped cube J8	C_{4v}	9.405	7.408
Johnson triangular cupola J3	C_{3v}	13.299	12.536
Heptagonal bipyramid	D_{7h}	13.556	11.103
Octagonal pyramid	C_{8v}	20.301	22.157
Enneagon	D_{9h}	33.133	30.777

Table S3. Selected bond distances (Å) and bond angles (°) in **1**.

Ce(1)-O(2)	2.356(2)	Ce(1)-O(7)	2.627(2)	Ce(2)-O(22)	2.581(3)
Ce(1)-O(3)	2.377(2)	Ce(1)-O(10)	2.632(2)	Ce(2)-O(19)	2.672(3)
Ce(1)-O(1)	2.388(2)	Ce(1)-O(8)	2.639(2)	Ce(2)-O(23)	2.618(3)
Ce(1)-O(11)	2.598(2)	Ce(2)-O(6)	2.378(2)	Ce(2)-O(20)	2.625(3)
Ce(1)-O(13)	2.599(3)	Ce(2)-O(5)	2.379(2)	Ce(2)-O(16)	2.639(3)
Ce(1)-O(14)	2.612(2)	Ce(2)-O(4)	2.388(2)	Ce(2)-O(17)	2.657(3)
O(2)-Ce(1)-O(3)	83.44(8)	O(13)-Ce(1)-O(10)	66.79(8)	O(11)-Ce(1)-O(10)	48.62(7)
O(2)-Ce(1)-O(1)	87.68(8)	O(14)-Ce(1)-O(10)	106.39(8)	O(22)-Ce(2)-O(20)	86.71(9)
O(3)-Ce(1)-O(1)	160.12(8)	O(7)-Ce(1)-O(10)	105.02(7)	O(23)-Ce(2)-O(20)	112.21(8)
O(2)-Ce(1)-O(11)	150.30(8)	O(2)-Ce(1)-O(8)	126.80(8)	O(6)-Ce(2)-O(16)	81.55(8)
O(3)-Ce(1)-O(11)	120.28(7)	O(3)-Ce(1)-O(8)	92.33(7)	O(5)-Ce(2)-O(16)	70.54(8)
O(1)-Ce(1)-O(11)	74.53(7)	O(1)-Ce(1)-O(8)	78.83(8)	O(4)-Ce(2)-O(16)	78.74(8)
O(2)-Ce(1)-O(13)	98.87(8)	O(11)-Ce(1)-O(8)	73.51(8)	O(22)-Ce(2)-O(16)	145.35(9)
O(3)-Ce(1)-O(13)	80.10(8)	O(13)-Ce(1)-O(8)	132.69(8)	O(23)-Ce(2)-O(16)	132.77(8)
O(1)-Ce(1)-O(13)	118.95(8)	O(14)-Ce(1)-O(8)	145.20(8)	O(20)-Ce(2)-O(16)	113.13(9)
O(11)-Ce(1)-O(13)	70.79(8)	O(7)-Ce(1)-O(8)	48.35(7)	O(6)-Ce(2)-O(17)	78.07(8)
O(2)-Ce(1)-O(14)	75.54(8)	O(10)-Ce(1)-O(8)	66.44(7)	O(5)-Ce(2)-O(17)	118.21(8)
O(3)-Ce(1)-O(14)	118.76(8)	O(6)-Ce(2)-O(5)	88.72(8)	O(4)-Ce(2)-O(17)	78.23(8)
O(1)-Ce(1)-O(14)	75.70(8)	O(6)-Ce(2)-O(4)	155.72(9)	O(22)-Ce(2)-O(17)	150.13(8)
O(11)-Ce(1)-O(14)	77.10(8)	O(5)-Ce(2)-O(4)	97.87(8)	O(23)-Ce(2)-O(17)	154.18(8)
O(13)-Ce(1)-O(14)	48.72(8)	O(6)-Ce(2)-O(22)	79.32(8)	O(20)-Ce(2)-O(17)	67.23(9)
O(2)-Ce(1)-O(7)	79.35(7)	O(5)-Ce(2)-O(22)	80.38(9)	O(16)-Ce(2)-O(17)	47.99(8)
O(3)-Ce(1)-O(7)	77.17(8)	O(4)-Ce(2)-O(22)	124.75(8)	O(6)-Ce(2)-O(19)	112.01(8)
O(1)-Ce(1)-O(7)	83.74(8)	O(6)-Ce(2)-O(23)	126.96(8)	O(5)-Ce(2)-O(19)	143.30(8)
O(11)-Ce(1)-O(7)	120.91(7)	O(5)-Ce(2)-O(23)	73.27(8)	O(4)-Ce(2)-O(19)	75.80(8)
O(13)-Ce(1)-O(7)	157.26(8)	O(4)-Ce(2)-O(23)	77.23(8)	O(22)-Ce(2)-O(19)	74.60(9)
O(14)-Ce(1)-O(7)	147.94(8)	O(22)-Ce(2)-O(23)	49.08(8)	O(23)-Ce(2)-O(19)	70.07(8)
O(2)-Ce(1)-O(10)	153.33(8)	O(6)-Ce(2)-O(20)	69.66(8)	O(20)-Ce(2)-O(19)	47.50(8)
O(3)-Ce(1)-O(10)	72.26(7)	O(5)-Ce(2)-O(20)	156.61(8)	O(16)-Ce(2)-O(19)	139.80(9)
O(1)-Ce(1)-O(10)	118.81(7)	O(4)-Ce(2)-O(20)	105.51(8)	O(17)-Ce(2)-O(19)	96.19(8)

Table S4. Hydrogen bonds for **1** [Å and °].

D-H...A	d(D-H)	d(H...A)	d(D...A)	<(DHA)
N(4)-H(4)...O(21)#3	0.78(3)	2.24(3)	2.994(4)	160(3)
N(10)-H(10)...O(12)#4	0.79(4)	2.15(4)	2.919(4)	164(4)
N(5)-H(5A)...O(15)#1	0.845(2)	2.17(2)	2.985(4)	163(3)
N(2)-H(2)...O(9)#5	0.848(2)	2.43(2)	3.194(4)	150(3)
N(1)-H(1)...O(8)	0.81(4)	2.37(4)	3.160(4)	165(3)
N(6)-H(6)...O(10)	0.78(3)	2.18(4)	2.905(4)	156(3)
N(13)-H(13)...O(16)	0.839(2)	2.34(3)	3.080(4)	147(3)
N(12)-H(12)...O(24)#2	0.79(4)	2.52(4)	3.288(5)	167(3)
N(14)-H(14)...O(17)	0.848(2)	2.24(2)	3.057(4)	162(4)

Symmetry transformations used to generate equivalent atoms:
#1 -x+1,y-1/2,-z+1/2 #2 -x+1,-y,-z #3 x,-y+1/2,z+1/2
#4 -x+1,-y+1,-z #5 -x+1/2,y+1/2,z

Table S5. SHAPE measures for seven co-ordinate La(III) center in **2**.[1]

Structure [CeO_9]	Symmetry	La1	La2
Muffin	C_s	2.877	4.492
Hula-hoop	C_{2v}	7.196	6.228
Tridiminished icosahedron J63	C_{3v}	12.733	10.6
Spherical tricapped trigonal prism	D_{3h}	4.724	5.345
Tricapped trigonal prism J51	D_{3h}	4.933	5.367
Spherical capped square antiprism	C_{4v}	3.535	5.077
Capped square antiprism J10	C_{4v}	4.378	6.062
Spherical-relaxed capped cube	C_{4v}	8.148	6.117
Capped cube J8	C_{4v}	9.48	7.376
Johnson triangular cupola J3	C_{3v}	13.291	12.611
Heptagonal bipyramid	D_{7h}	13.434	11.123
Octagonal pyramid	C_{8v}	20.005	22.289
Enneagon	D_{9h}	33.186	30.885

Table S6. Selected bond distances (Å) and bond angles (°) in **2**.

La(1)-O(1)	2.411(8)	La(1)-O(14)	2.653(10)	La(2)-O(22)	2.622(9)
La(1)-O(3)	2.415(8)	La(1)-O(10)	2.684(9)	La(2)-O(20)	2.627(9)
La(1)-O(2)	2.418(8)	La(1)-O(13)	2.691(9)	La(2)-O(23)	2.633(9)
La(1)-O(7)	2.614(10)	La(2)-O(5)	2.390(9)	La(2)-O(19)	2.655(9)
La(1)-O(11)	2.630(10)	La(2)-O(4)	2.396(8)	La(2)-O(17)	2.657(9)
La(1)-O(8)	2.640(9)	La(2)-O(6)	2.409(8)	La(2)-O(16)	2.668(9)
O(1)-La(1)-O(3)	155.5(3)	O(7)-La(1)-O(10)	75.2(3)	O(6)-La(2)-O(23)	117.6(3)
O(1)-La(1)-O(2)	88.8(3)	O(11)-La(1)-O(10)	47.1(3)	O(22)-La(2)-O(23)	48.2(3)
O(3)-La(1)-O(2)	97.7(3)	O(8)-La(1)-O(10)	70.4(3)	O(20)-La(2)-O(23)	77.6(3)
O(1)-La(1)-O(7)	78.8(3)	O(14)-La(1)-O(10)	139.7(3)	O(5)-La(2)-O(19)	153.6(3)
O(3)-La(1)-O(7)	125.6(3)	O(1)-La(1)-O(13)	78.2(3)	O(4)-La(2)-O(19)	118.8(3)
O(2)-La(1)-O(7)	80.6(3)	O(3)-La(1)-O(13)	77.8(3)	O(6)-La(2)-O(19)	72.5(3)
O(1)-La(1)-O(11)	69.7(3)	O(2)-La(1)-O(13)	118.0(3)	O(22)-La(2)-O(19)	66.1(3)
O(3)-La(1)-O(11)	105.3(3)	O(7)-La(1)-O(13)	149.9(3)	O(20)-La(2)-O(19)	48.2(3)
O(2)-La(1)-O(11)	157.0(3)	O(11)-La(1)-O(13)	67.0(3)	O(23)-La(2)-O(19)	106.2(3)
O(7)-La(1)-O(11)	86.9(3)	O(8)-La(1)-O(13)	154.0(3)	O(5)-La(2)-O(17)	127.0(3)
O(1)-La(1)-O(8)	126.9(3)	O(14)-La(1)-O(13)	48.2(3)	O(4)-La(2)-O(17)	78.6(3)
O(3)-La(1)-O(8)	77.5(3)	O(10)-La(1)-O(13)	95.7(3)	O(6)-La(2)-O(17)	93.0(3)
O(2)-La(1)-O(8)	73.7(3)	O(5)-La(2)-O(4)	87.5(3)	O(22)-La(2)-O(17)	131.6(3)
O(7)-La(1)-O(8)	49.5(3)	O(5)-La(2)-O(6)	83.3(3)	O(20)-La(2)-O(17)	73.0(3)
O(11)-La(1)-O(8)	112.2(3)	O(4)-La(2)-O(6)	160.1(3)	O(23)-La(2)-O(17)	145.5(3)
O(1)-La(1)-O(14)	81.6(3)	O(5)-La(2)-O(22)	100.1(3)	O(19)-La(2)-O(17)	66.2(3)
O(3)-La(1)-O(14)	78.5(3)	O(4)-La(2)-O(22)	118.6(3)	O(5)-La(2)-O(16)	79.7(3)
O(2)-La(1)-O(14)	70.0(3)	O(6)-La(2)-O(22)	80.5(3)	O(4)-La(2)-O(16)	83.9(3)
O(7)-La(1)-O(14)	144.8(3)	O(5)-La(2)-O(20)	150.6(3)	O(6)-La(2)-O(16)	77.2(3)
O(11)-La(1)-O(14)	113.1(3)	O(4)-La(2)-O(20)	75.0(3)	O(22)-La(2)-O(16)	157.6(3)
O(8)-La(1)-O(14)	132.8(3)	O(6)-La(2)-O(20)	120.1(3)	O(20)-La(2)-O(16)	120.5(3)
O(1)-La(1)-O(10)	111.6(3)	O(22)-La(2)-O(20)	69.6(3)	O(23)-La(2)-O(16)	148.8(3)
O(3)-La(1)-O(10)	76.2(3)	O(5)-La(2)-O(23)	75.4(3)	O(19)-La(2)-O(16)	104.4(3)
O(2)-La(1)-O(10)	144.0(3)	O(4)-La(2)-O(23)	76.6(3)	O(17)-La(2)-O(16)	48.3(3)

Table S7. Hydrogen bonds for **2** [Å and °].

D-H...A	d(D-H)	d(H...A)	d(D...A)	<(DHA)
N(3)-H(3)...O(9)#1	1.06(12)	2.22(13)	3.248(15)	162(10)
N(11)-H(11)...O(18)#3	0.88	2.44	3.163(14)	139.4
N(14)-H(14)...O(19)	0.88	2.27	2.915(14)	130.1
N(10)-H(10)...O(17)	0.87(2)	2.41(13)	3.147(14)	143(18)
N(13)-H(13)...O(12)	0.87(2)	2.21(5)	3.005(15)	151(10)
N(2)-H(2)...O(13)	0.99(13)	2.10(13)	3.064(14)	164(10)
N(4)-H(4)...O(14)	0.75(16)	2.36(17)	3.076(16)	162(18)
N(15)-H(15A)...O(24)#2	0.93(15)	2.14(15)	2.993(14)	152(13)
N(5)-H(5A)...O(21)#2	0.88	2.35	2.918(14)	122.1

Symmetry transformations used to generate equivalent atoms:

#1 -x+1,-y+2,-z+1 #2 -x+1,y-1/2,-z+3/2 #3 -x+3/2,y+1/2,z

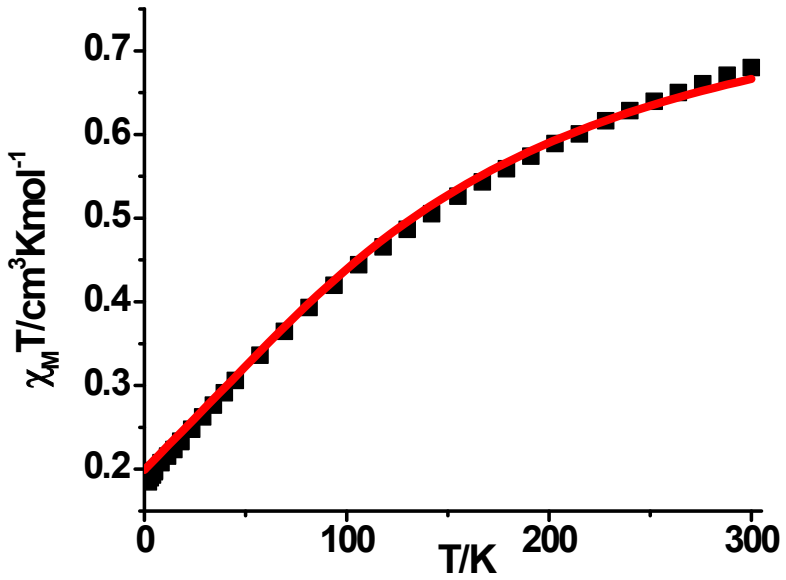

Figure S1. Experimental and *ab inito* CASSCF computed temperature dependence of the $\chi_M T$ product at 1000 Oe for **1**. Black squares correspond to the experimental magnetic susceptibility data for **1**. The solid lines are the computed magnetic susceptibilities. The computed susceptibilities are multiplied by a factor of 0.986.

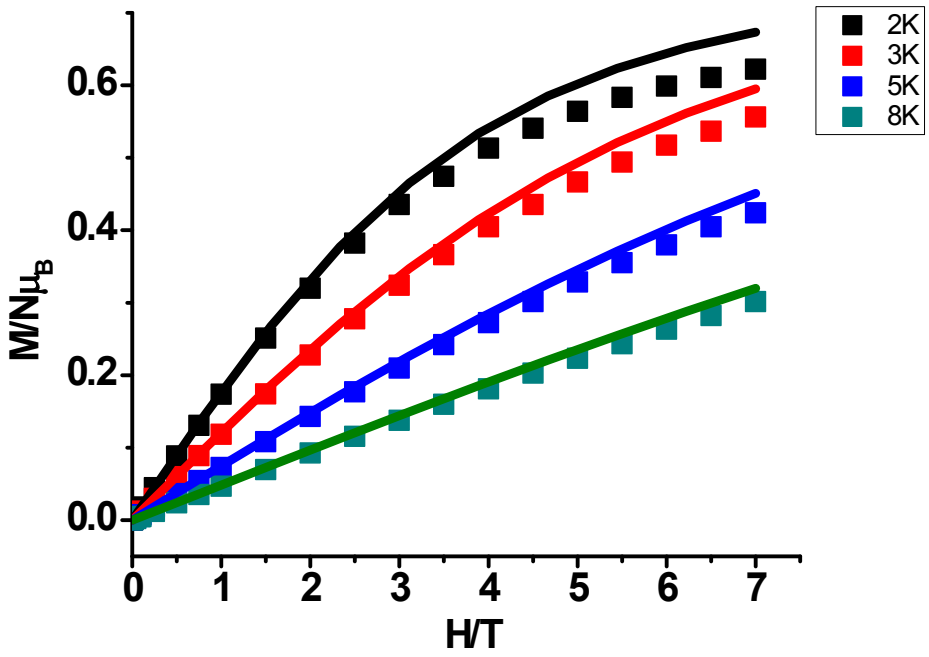

Figure S2. The field-dependent magnetization data for **1**. Black squares correspond to the experimental magnetic susceptibility data for **1**. The solid lines are the computed magnetic susceptibilities. The computed susceptibilities are multiplied by a factor of 0.98.

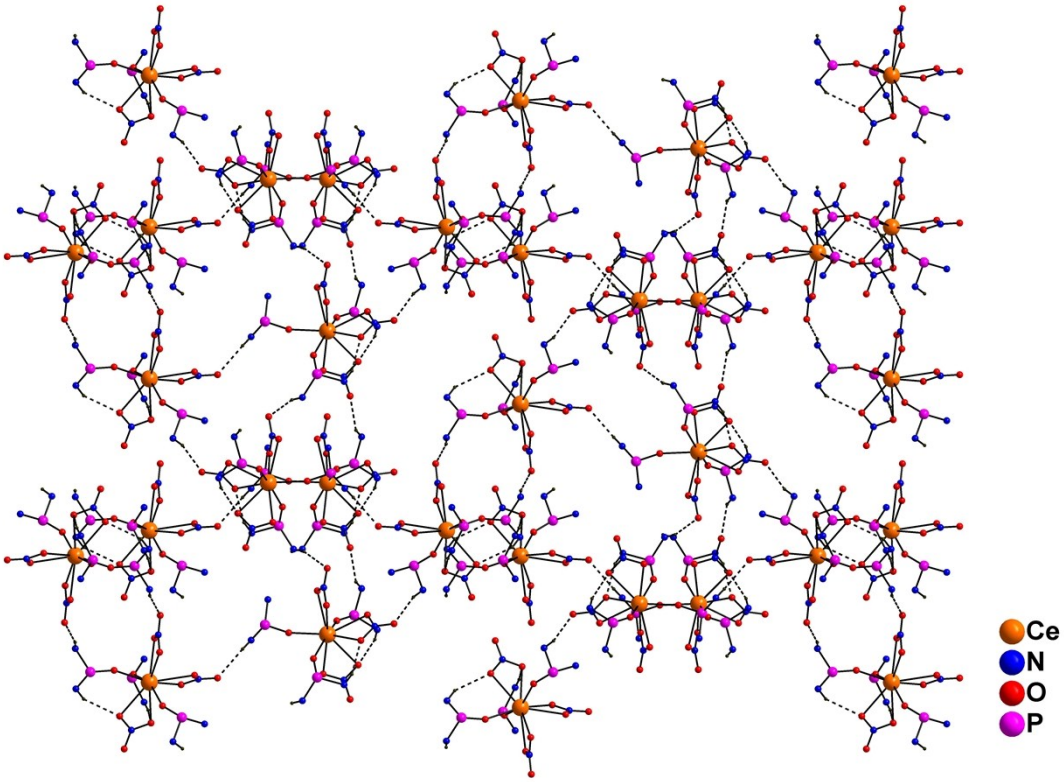

Figure S3. H-bonding pattern in complex **1** leading to formation of a network of monomeric cerium(III) complexes.

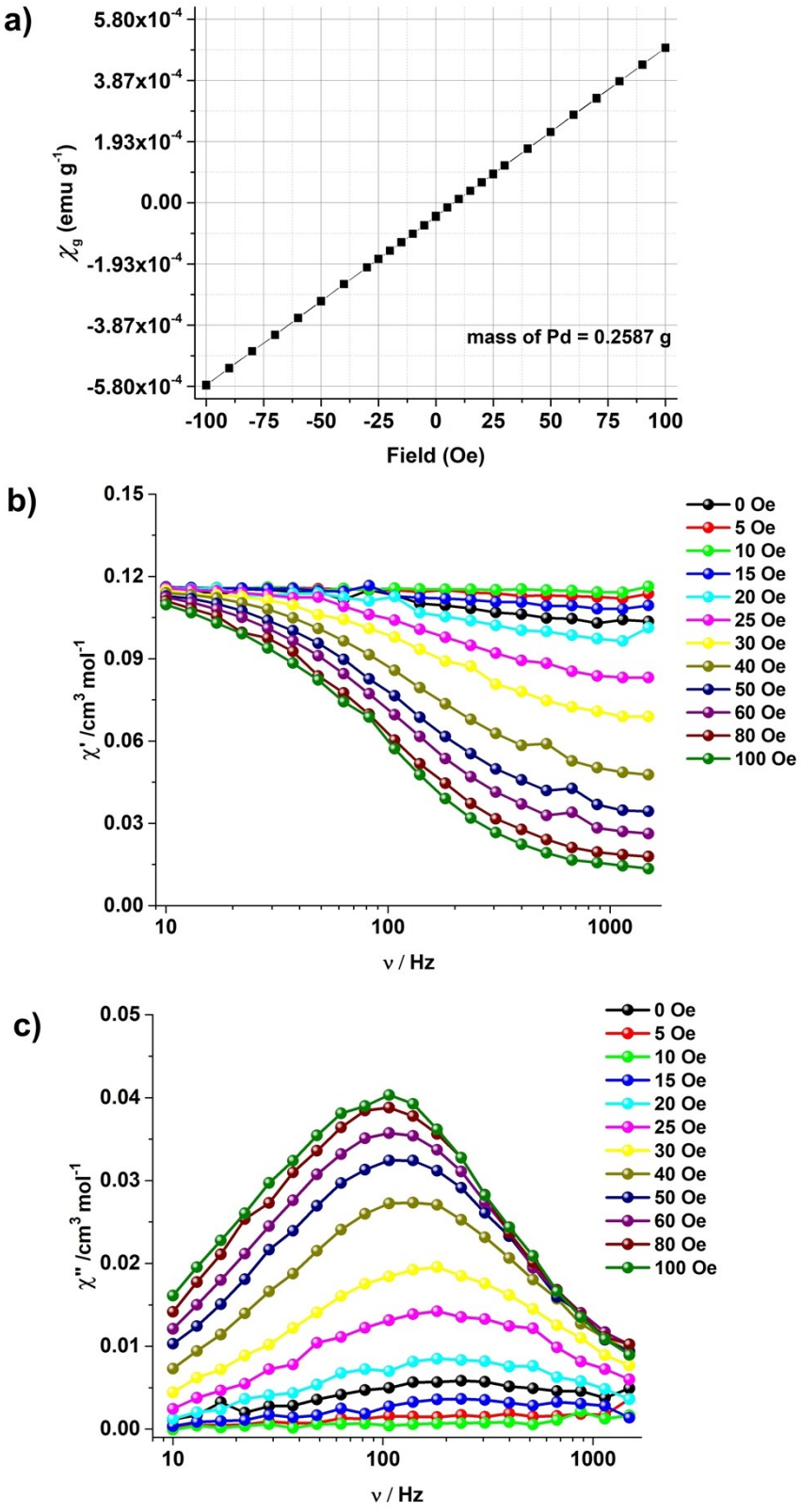

Figure S4. (a) Field dependence of the susceptibility of standard Pd sample measured at 298 K in first MPMS indicating a remnant dc field ~ 8.5 Oe. (b) Frequency dependence of the (a) in-phase (χ_M') component and (b) out-of-phase (χ_M'') component of the ac susceptibility measured in an oscillating ac field of 3.5 Oe under various dc fields for complex **1**.

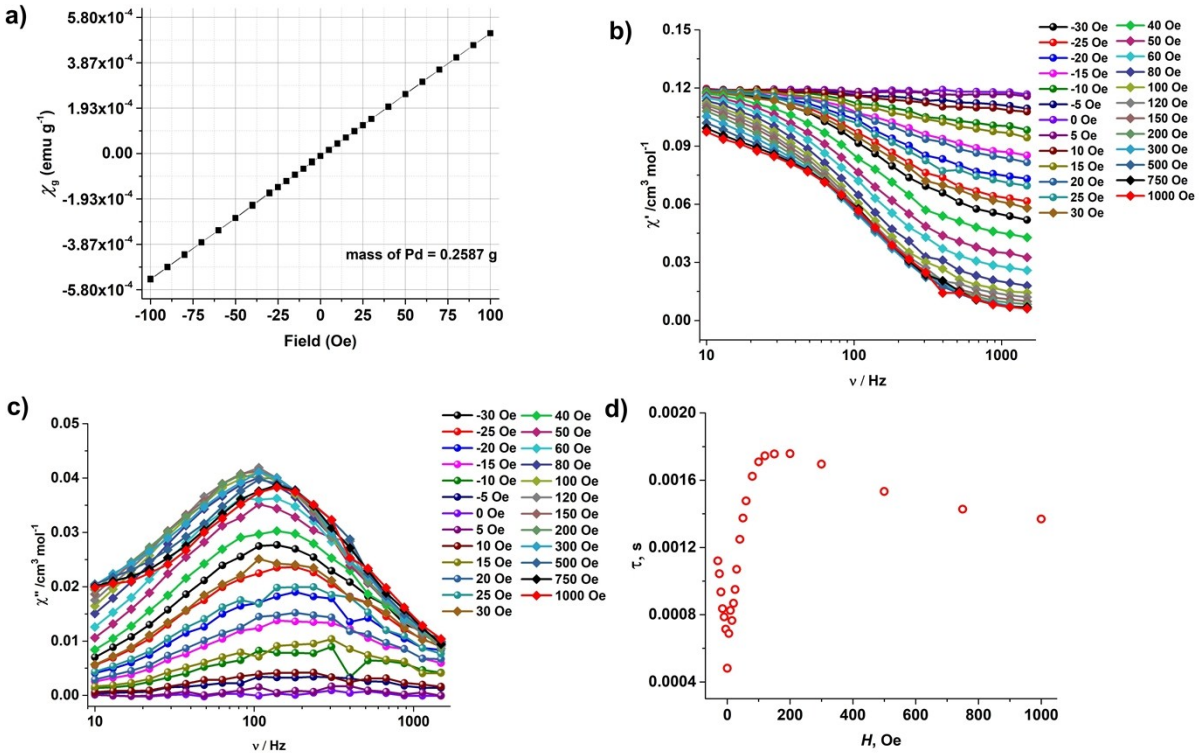

Figure S5. (a) Field dependence of the susceptibility of standard Pd sample measured at 298 K in second MPMS indicating a remnant dc field ~ 2 Oe. (b) Frequency dependence of the (a) in-phase (χ_M') component and (b) out-of-phase (χ_M'') component of the ac susceptibility measured in an oscillating ac field of 3.5 Oe under various dc fields for complex **1**. (d) Field dependence of the relaxation time at various dc fields for complex **1**.

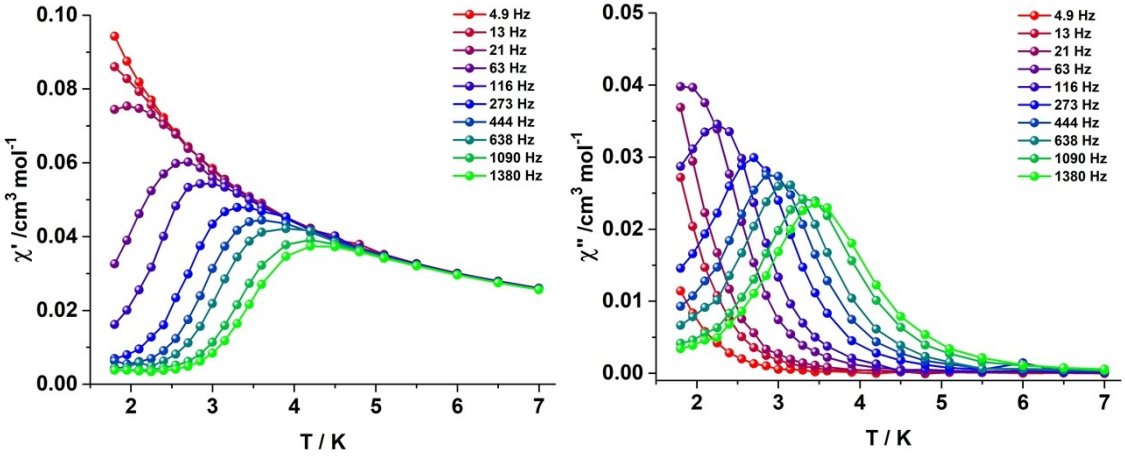

Figure S6. Temperature dependence of the (left) in-phase (χ_M') component and (right) out-of-phase (χ_M'') component of the ac susceptibility measured in an oscillating ac field of 3.5 Oe for complex **1** at various ac frequencies under an applied dc field of 200 Oe.

Table S8. Best-fit parameters obtained from the least-square fitting of the frequency dependent ac susceptibility data of complex **1** at an applied dc field of 200 Oe based on generalized Debye model considering one relaxation.

T (K)	χ_S (cm^3 mol^{-1})	χ_T (cm^3 mol^{-1})	τ (s)	α
1.8	3.66E-03	9.63E-02	3.90E-03	4.23E-02
1.95	3.49E-03	8.89E-02	3.01E-03	3.56E-02
2.1	3.33E-03	8.26E-02	2.28E-03	3.04E-02
2.25	3.30E-03	7.76E-02	1.76E-03	2.27E-02
2.4	3.05E-03	7.26E-02	1.27E-03	2.24E-02
2.55	2.89E-03	6.84E-02	9.17E-04	2.04E-02
2.7	2.82E-03	6.45E-02	6.59E-04	1.48E-02
2.85	2.46E-03	6.13E-02	4.76E-04	1.78E-02
3	2.37E-03	5.82E-02	3.46E-04	1.40E-02
3.15	2.28E-03	5.55E-02	2.54E-04	1.45E-02
3.3	2.02E-03	5.31E-02	1.87E-04	1.34E-02
3.45	1.51E-03	5.08E-02	1.39E-04	1.79E-02
3.6	1.13E-03	4.88E-02	1.05E-04	1.87E-02

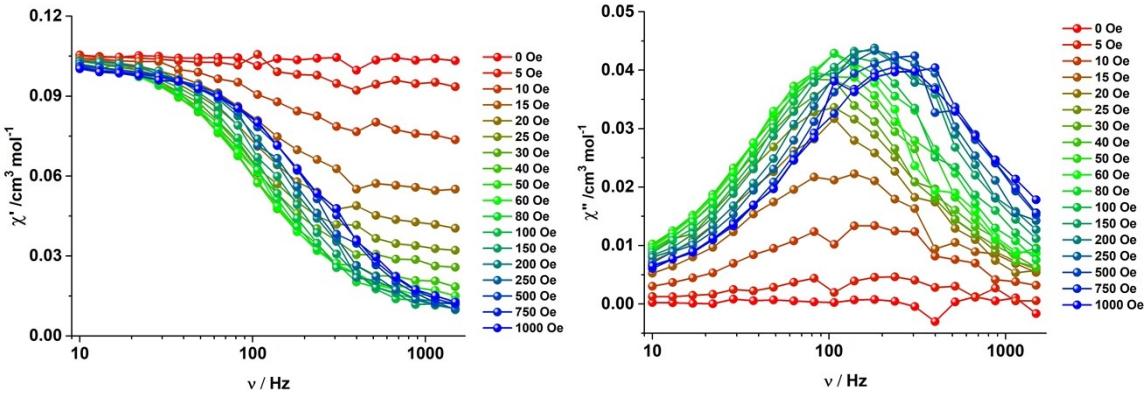

Figure S7. Frequency dependence of the (left) in-phase (χ_M') component and (right) out-of-phase (χ_M'') component of the ac susceptibility measured in an oscillating ac field of 3.5 Oe for complex **1@2** at various dc fields.

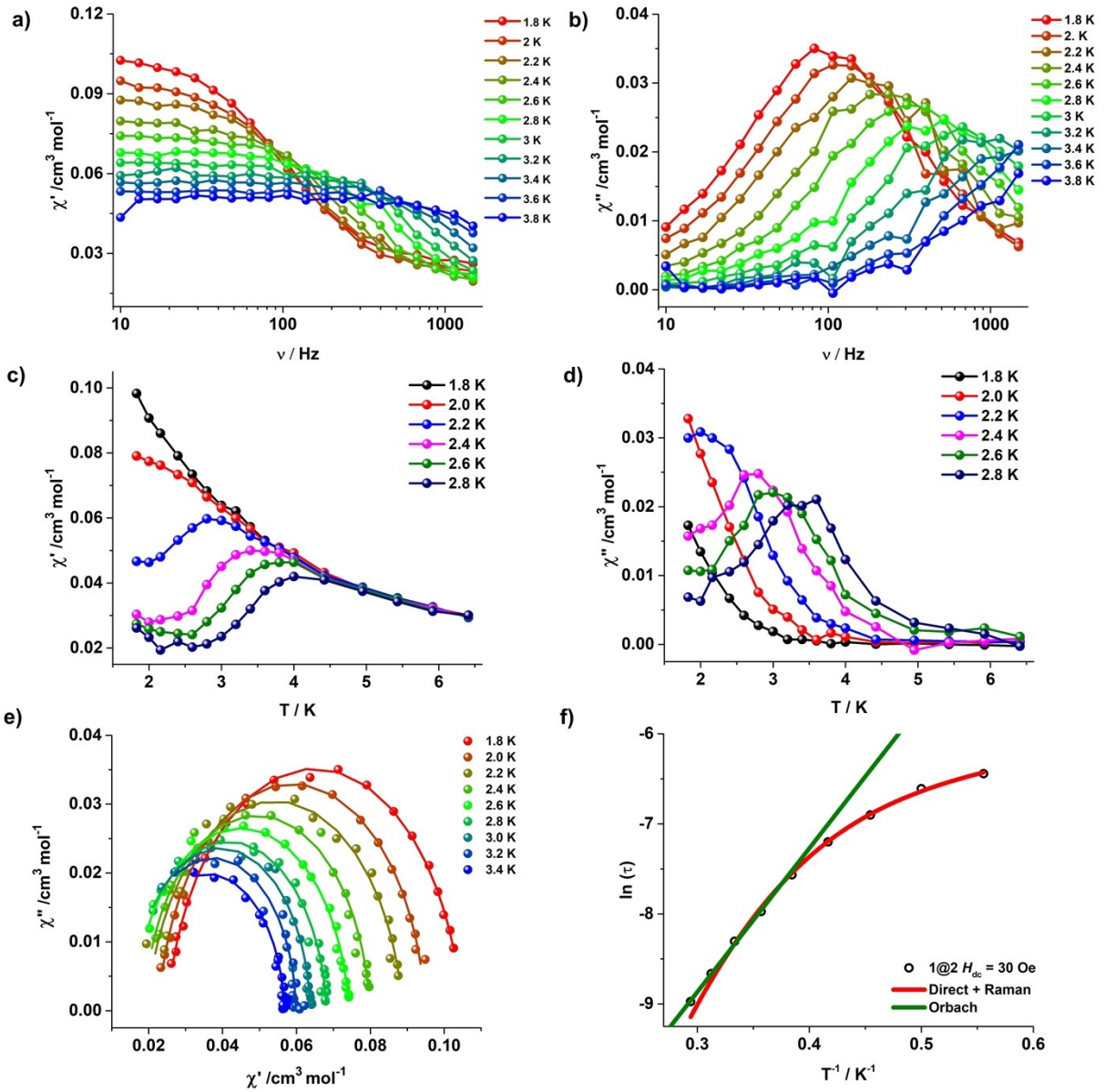

Figure S8. Frequency dependence of the (a) in-phase (χ_M') component and (b) out-of-phase (χ_M'') of the ac susceptibility measured in an oscillating ac field of 3.5 Oe for complex **1@2** at an applied dc field of 30 Oe. Temperature dependence of the (c) in-phase (χ_M') component and (d) out-of-phase (χ_M'') of the ac susceptibility measured in an oscillating ac field of 3.5 Oe for complex **1@2** at an applied dc field of 30 Oe. (e) Cole–Cole plot for **1@2** under an applied dc field of 30 Oe. Solid black lines are the best fit to the Debye model. (f) Plot of the relaxation time τ versus T^{-1} obtained for **1@2** under an applied dc field of 30 Oe. Solid lines are best fits to the multiple relaxation processes. ($D = 306.5\ s^{-1}\ K^{-1}$, $C = 0.80\ s^{-1}\ K^{-n}$ and $n = 7.55$)

Table S9. Best-fit parameters obtained from the least-square fitting of the frequency dependent ac susceptibility data of complex **1@2** at an applied dc field of 30 Oe based on generalized Debye model considering one relaxation.

T (K)	χ_S (cm^3 mol^{-1})	χ_T (cm^3 mol^{-1})	τ (s)	α
1.8	2.51E-02	1.05E-01	1.59E-03	7.87E-02
2	2.28E-02	9.49E-02	1.35E-03	5.66E-02
2.2	1.97E-02	8.88E-02	1.01E-03	8.06E-02
2.4	1.88E-02	7.98E-02	7.47E-04	4.58E-02
2.6	1.59E-02	7.42E-02	5.18E-04	6.01E-02
2.8	1.50E-02	6.82E-02	3.44E-04	5.02E-02
3	1.52E-02	6.36E-02	2.47E-04	1.53E-02
3.2	1.49E-02	5.98E-02	1.73E-04	6.74E-03
3.4	1.53E-02	5.67E-02	1.27E-04	2.57E-02

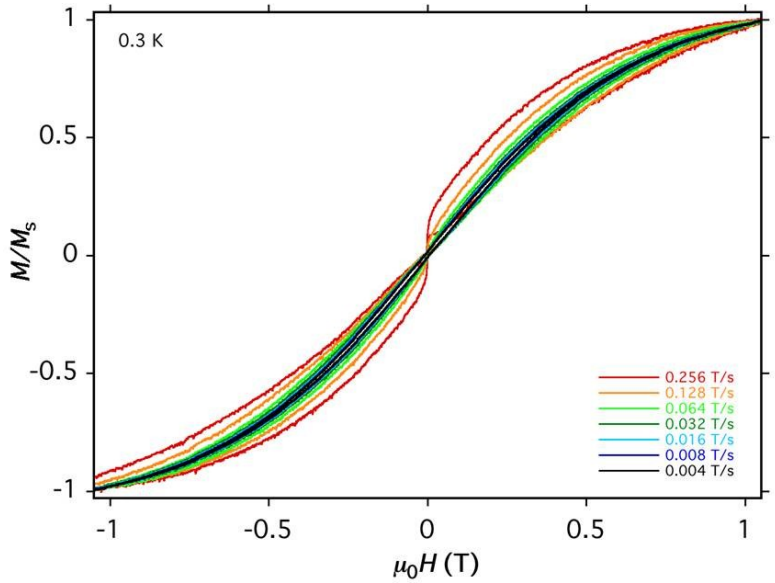

Figure S9. Normalized field-dependent magnetization data performed with oriented crystals of **1**, aligned with the transverse field method at 0.3 K with varying field sweep rates.

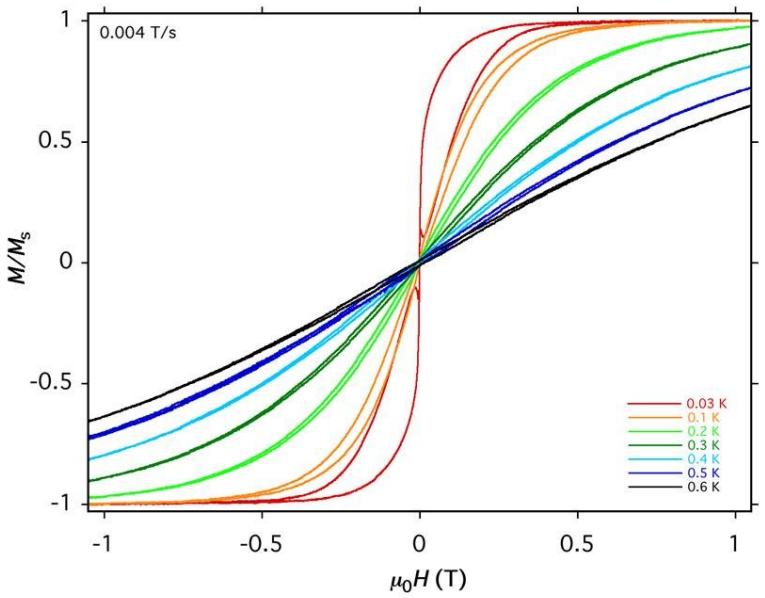

Figure S10. Normalized field-dependent magnetization data performed with oriented crystals of **1**, aligned with the transverse field method at varying temperatures with field sweep rates of 0.004 T/s.

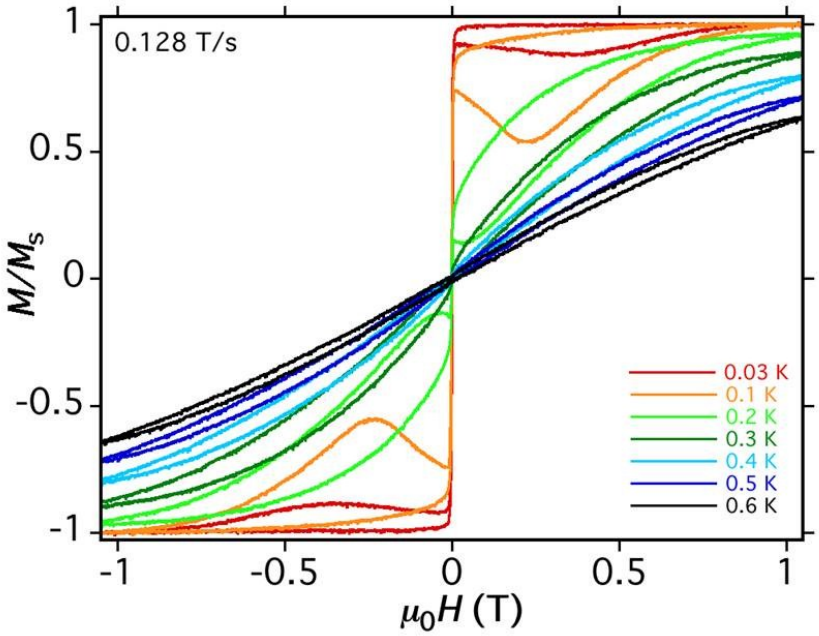

Figure S11. Normalized field-dependent magnetization data performed with oriented crystals of **1**, aligned with the transverse field method at varying temperatures with field sweep rates of 0.128 T/s.

Table S10: SINGLE_ANISO computed spectrum, *g*-tensors, relative energies and angles (q) of the principal anisotropy axes of the first excited states with respect to the ground state, for ground and excited state Kramers doublets.

Levels	Energy (cm^{-1})	g_{zz}	g_{xx}	g_{yy}	Angles between g_{zz} axis
1					
1	0.000	0.26	1.90	1.67	–
2	0.000				
3	220.13	2.99	0.95	1.57	16.57
4	220.13				
1'					
1	0.000	0.01	1.98	1.68	–
2	0.000				
3	220.13	1.16	2.35	2.02	109.11
4	220.13				
1a					
1	0.000	4.15	0.08	0.13	-
2	0.000				
3	687.06	2.26	0.61	0.91	4.23
4	687.06				
1b					
1	0.000	4.14	0.0	0.0	-
2	0.000				
3	1123.94	2.25	0.19	0.21	0.90
4	1123.94				
5	2275.62	8.0	0.0	0.0	0.13
6	2275.62				
7	2394.43	0.46	2.73	2.17	0.21
8	2394.43				

Table S11: Composition of wave functions of the ground state of Ce(III) for complex **1** as derived from SINGLE_ANISO calculations.

w.f.	m_J	c_i		w.f.	m_J	c_i	
		real	imag			real	imag
1	-5/2	-0.399727	-0.283782	2	-5/2	0.025256	0.01793
	-3/2	0.100134	-0.129129		-3/2	-0.067674	-0.43807
	-1/2	0.01013	0.21647		-1/2	-0.648621	0.260517
	1/2	0.378079	0.587907		1/2	0.133572	-0.170647
	3/2	-0.308775	0.31803		3/2	-0.006899	-0.163259
	5/2	-0.030974	0		5/2	-0.490218	0
3	-5/2	-0.810822	0.195998	4	-5/2	0.000001	0
	-3/2	-0.005502	0.313408		-3/2	0.084862	0.262004
	-1/2	-0.214903	0.004294		-1/2	0.269028	-0.107105
	1/2	-0.286662	-0.040896		1/2	-0.209896	0.04632
	3/2	0.020926	-0.274608		3/2	0.078986	0.303342
	5/2	-0.000001	0		5/2	-0.834175	0

Table S12: CASSCF computed Mulliken charges.

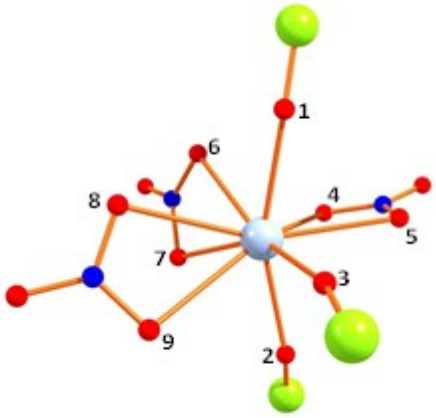

Atom label	**1**	**1'**	**1a**	**1b**
O1	-1.3205	-1.3190	-1.3027	-1.2749
O2	-1.3395	-1.3444	-1.3245	-1.2878
O3	-1.3292	-1.3166	-1.3039	–
O4	-0.8752	-0.8867	–	–
O5	-0.8874	-0.8926	–	–
O6	-0.8694	-0.8805	–	–
O7	-0.8730	-0.8734	–	–
O8	-0.8354	-0.8548	–	–
O9	-0.8938	-0.8562	–	–

Table S13: Composition of wave functions of the ground state of Ce(III) for complex **1'** as derived from SINGLE_ANISO calculations.

w.f.	m_J	c_i		w.f.	m_J	c_i	
		real	imag			real	imag
1	-5/2	-0.279532	0.041097	2	-5/2	-0.340761	0.050099
	-3/2	-0.178578	0.475703		-3/2	0.240624	-0.341835
	-1/2	0.046462	0.3979		-1/2	-0.323156	0.322021
	1/2	-0.366559	-0.271591		1/2	0.011909	0.400426
	3/2	-0.287787	-0.303199		3/2	-0.245873	-0.444669
	5/2	-0.344424	0		5/2	0.282537	0
3	-5/2	0.080709	-0.734356	4	-5/2	0.01034	-0.094079
	-3/2	-0.325287	0.168848		-3/2	0.093207	-0.303607
	-1/2	0.12756	-0.034579		-1/2	-0.436844	-0.041994
	1/2	-0.005981	0.438817		1/2	-0.048308	0.123019
	3/2	-0.311972	0.059481		3/2	-0.203374	0.304894
	5/2	0.094646	0		5/2	-0.738778	0

Table S14: Composition of wave functions of the ground state of Ce(III) for complex **1a** as derived from SINGLE_ANISO calculations.

w.f.	m_J	c_i		w.f.	m_J	c_i	
		real	imag			real	imag
1	-5/2	0.719415	-0.683569	2	-5/2	0	0
	-3/2	-0.010063	-0.016311		-3/2	0.01305	-0.028737
	-1/2	-0.099658	0.062178		-1/2	0.00256	0.002742
	1/2	-0.000033	-0.003751		1/2	0.115075	-0.023571
	3/2	-0.029255	-0.011843		3/2	0.00394	0.018756
	5/2	0	0		5/2	-0.992383	0
3	-5/2	0.010422	-0.024406	4	-5/2	0.001124	-0.002633
	-3/2	0.531524	0.30637		-3/2	0.217754	0.740072
	-1/2	-0.121759	-0.048698		-1/2	0.040765	0.094473
	1/2	-0.070873	-0.074592		1/2	0.003032	-0.131101
	3/2	0.595094	0.490904		3/2	-0.073012	-0.609139
	5/2	0.002863	0		5/2	-0.026538	0

Table S15: Composition of wave functions of the ground state of Ce(III) for complex **1b** as derived from SINGLE_ANISO calculations.

w.f.	m_J	c_i		w.f.	m_J	c_i	
		real	imag			real	imag
1	-5/2	0.000148	-0.001041	2	-5/2	0	0
	-3/2	-0.961719	-0.227984		-3/2	0.028913	0.149235
	-1/2	0.001823	-0.002827		-1/2	-0.001092	0.000035
	1/2	-0.000188	0.001076		1/2	-0.003055	0.001407
	3/2	0.143688	0.049606		3/2	0.090517	0.984218
	5/2	0	0		5/2	-0.001051	0
3	-5/2	-0.000592	-0.001976	4	-5/2	0	0
	-3/2	0.003276	-0.001302		-3/2	0.000303	0.000029
	-1/2	-0.033631	-0.988143		-1/2	-0.129429	-0.075329
	1/2	0.109279	0.102394		1/2	-0.95629	0.251129
	3/2	0.000114	0.000282		3/2	0.000308	-0.003512
	5/2	0	0		5/2	-0.002063	0

References

1. M. Llunell, D. Casanova, J. Cirera, J. Bofill, P. Alemany and S. Alvarez, *SHAPE (version 2.1)*, Barcelona, **2013**.